nature geoscience

ARTICLES

PUBLISHED ONLINE: 5 JUNE 2017 | DOI: 10.1038/NGEO2963

Hotspots of soil N_2O emission enhanced through water absorption by plant residue

A. N. Kravchenko[1]*, E. R. Toosi[1], A. K. Guber[1], N. E. Ostrom[2], J. Yu[3], K. Azeem[4], M. L. Rivers[5] and G. P. Robertson[1,6]

N_2O is a highly potent greenhouse gas and arable soils represent its major anthropogenic source. Field-scale assessments and predictions of soil N_2O emission remain uncertain and imprecise due to the episodic and microscale nature of microbial N_2O production, most of which occurs within very small discrete soil volumes. Such hotspots of N_2O production are often associated with decomposing plant residue. Here we quantify physical and hydrological soil characteristics that lead to strikingly accelerated N_2O emissions in plant residue-induced hotspots. Results reveal a mechanism for microscale N_2O emissions: water absorption by plant residue that creates unique micro-environmental conditions, markedly different from those of the bulk soil. Moisture levels within plant residue exceeded those of bulk soil by 4–10-fold and led to accelerated N_2O production via microbial denitrification. The presence of large ($\varnothing > 35$ μm) pores was a prerequisite for maximized hotspot N_2O production and for subsequent diffusion to the atmosphere. Understanding and modelling hotspot microscale physical and hydrologic characteristics is a promising route to predict N_2O emissions and thus to develop effective mitigation strategies and estimate global fluxes in a changing environment.

Extremely high temporal and spatial variability of N_2O fluxes is one of the main reasons for persistent difficulties in curbing uncertainties in N_2O fluxes[1,2], especially from arable soils that are responsible for the majority of anthropogenic N_2O emissions[3–6]. Despite substantial research efforts[7–9], accuracy in predicting N_2O production and emission, either via empirical or process-based models, remains surprisingly low[9]. While the Intergovernmental Panel on Climate Change has recently proposed a closed global budget for N_2O, there remains enormous uncertainty regarding precise source and sink terms[10,11]. Soil N_2O fluxes measured simultaneously within several metres of one another often differ by a factor of 2 or more[12] and day-to-day fluxes can change by an order of magnitude or more[13], requiring intensive sampling regimes to accurately estimate annual fluxes[14]. Uncertainties associated with predicting N_2O emissions from agricultural soils amended with plant residues, as happens, for example, with cover crops, green manure, and land conversion[3,15], can be particularly high[3–6].

At least some of this variability arises because the majority of N_2O production in soil occurs within very small soil volumes (<1 cm^3), so-called hotspots, and typically persists for very short periods of <2 weeks[16]. Hotspots can develop around plant residues, fragments of particulate organic matter, plant roots or inside soil aggregates[17–20]. Plant residues appear to be particularly potent N_2O sources: in one early experiment more than 80% of the N_2O produced in a soil core was traced to an 80 mg plant leaf remnant[19]. The factors that activate such high microscale emissions are poorly known but could be crucial for understanding and mitigating N_2O fluxes. There is growing acknowledgement that a failure to understand the mechanisms that control the occurrence and activities of hotspots is a main reason for difficulties in predicting N_2O emissions, and that without considering microscale processes, accurate large-scale predictions will remain an intractable problem[1,21].

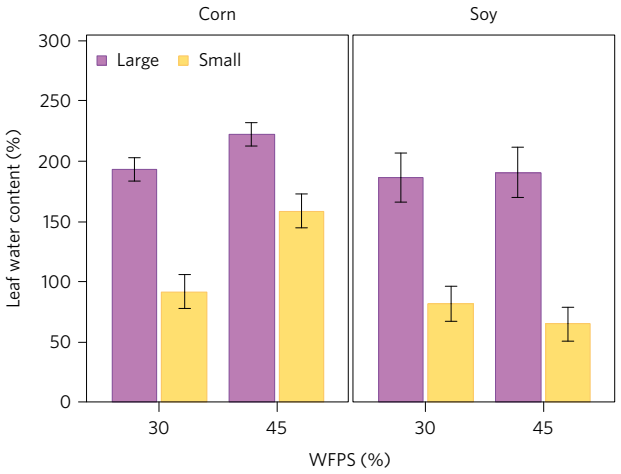

Figure 1 | Gravimetric moisture content of corn and soybean leaves used in the incubations. Means and error bars (s.e.m.); the differences between small- and large-pore treatments within each plant type and each WFPS level were statistically significant at $p < 0.01$ ($n = 3$).

Here we assess how factors known to influence overall N_2O emissions[22,23], specifically plant residue quality, soil moisture, and soil pore size distribution (PSD), synergistically affect microscale N_2O production and emissions. We examined N_2O emissions for 110 days in microcosms constructed from soil dominated by either small (<10 μm) or large (>35 μm) pores. Microcosms were assigned to one of two plant residue treatments (corn or soybean leaf discs), or to a control without residues, and were incubated at low (30%) or high (45%) water-filled pore space (WFPS). X-ray computed

[1]Department of Plant, Soil and Microbial Sciences, Michigan State University, East Lansing, Michigan 48824, USA. [2]Department of Integrative Biology and DOE Great Lakes Bioenergy Research Institute, Michigan State University, East Lansing, Michigan 48824, USA. [3]Faculty of Resources and Environmental Science, Hubei University, Wuhan 430052, China. [4]Department of Agronomy, The University of Agriculture, Peshawar 25130, Khyber Pakhtunkhwa, Pakistan. [5]Center for Advanced Radiation Sources, The University of Chicago, Argonne National Lab, Argonne, Illinois 60439, USA. [6]W. K. Kellogg Biological Station, Michigan State University, Hickory Corners, Michigan 49060, USA. *e-mail: kravche1@msu.edu

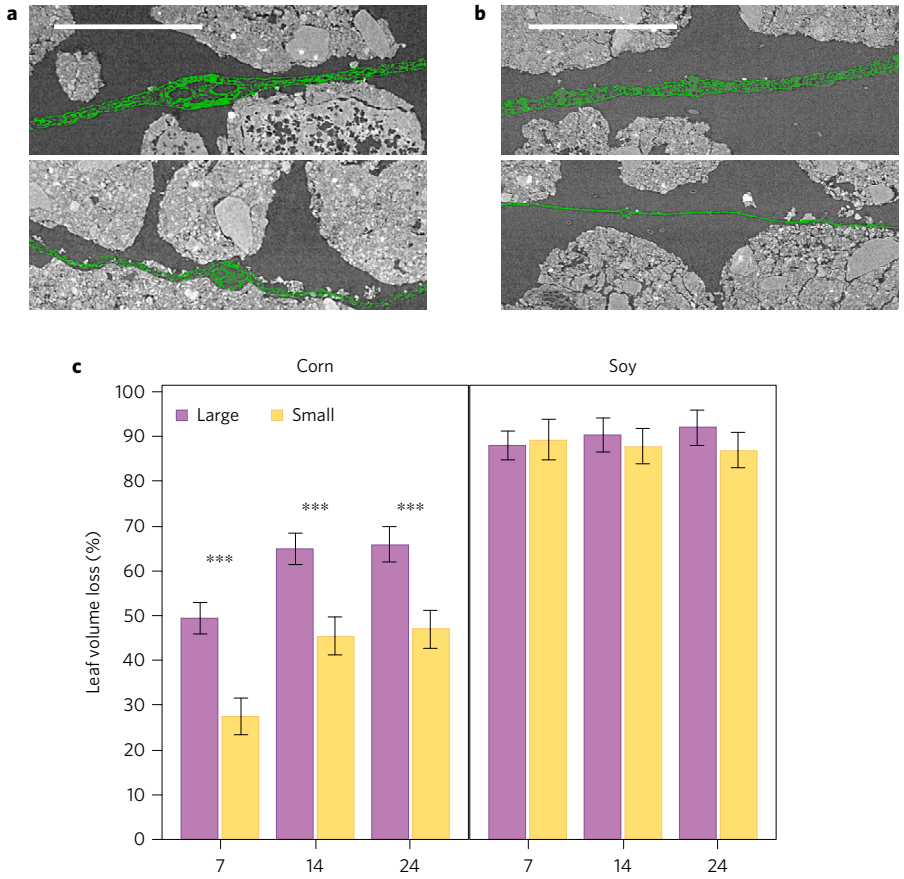

Figure 2 | Decomposition of added plant residue. a,**b**, X-ray μ-CT images of corn (**a**) and soybean leaves (**b**) (green) at the start of the incubation experiments (top) and after 7 days of incubation (bottom). Scale bars, 1 mm. **c**, Loss in leaf volume during the incubation determined from the X-ray μ-CT images. Data are means for plant residue type and pore sizes averaged across both levels of WFPS and agricultural managements, error bars indicate s.e.m. ($n = 4$), asterisks indicate significant differences between pore sizes at $p < 0.001$.

micro-tomography (X-ray μ-CT) provided unique high-resolution *in situ* characterization of plant residue decomposition dynamics and soil PSDs[24–26]. X-ray μ-CT also facilitated visualization of water within the microcosms; and optical oxygen sensors enabled microscale 2D mapping of O_2 distributions. Site-preference analysis (SP: the difference in $\delta^{15}N$ between the central and outer N atoms in N_2O) provided knowledge of alternative microbial pathways of N_2O production and, in particular, distinguished microbial production via bacterial denitrification versus nitrification and fungal denitrification[27,28].

Consistent with previous studies[1,19], our results demonstrate that N_2O hotspots of small (sub-centimetre) size can be a source of substantial N_2O emissions. We determined that two co-occurring physical conditions are necessary for the occurrence of a highly potent hotspot: the presence of a spatially aggregated source of organic material and the presence of large pores in its vicinity.

Micro-environments within plant residue hotspots

Spatially aggregated sources of organic material, that is, intact pieces of plant leaves, as in our study, aggregated clumps of ground plant residue[29–31], or topical inputs of animal manure[32] are known to foster extraordinarily high N_2O emissions. Moreover, the greater the spatial aggregation of the plant residue the greater the N_2O emissions that can be expected[30]. Our results, for the first time, demonstrate that an important underlying reason for this phenomenon is absorption of water from the surrounding soil by the residue. Even at the low soil water contents of our experiment, that is, 15% and 24% by mass (Supplementary Table 1), gravimetric water contents of incubated leaf residue fragments were in the 60–220% range (Fig. 1). Essentially, the plant residue remnants within the soil matrix served as a sponge that accumulated water and thus, even in a relatively dry soil, acted as a local spot of high moisture for microbial heterotrophs. Very fine pores of the plant residue extract and retain water even from moderately dry soil due to strong capillary forces.

Pore size distributions of the surrounding soil affect how much water can be absorbed by the residue (Fig. 1): when the residue is surrounded by large soil pores (Fig. 2a,b) it retains substantially more water, leading to its faster decomposition (Fig. 2c), than when it is in contact with small pores. In the latter case more soil water is retained by the small pores within the soil matrix, rather than in the residue. Both corn and soybean residue absorbed comparable amounts of water, suggesting the general nature of this phenomenon.

Local anoxia within plant residues and denitrification

The conventional expectation is that most N_2O production by denitrification occurs at relatively high soil moisture levels (60–90% WFPS), while that produced by nitrification prevails at lower moisture contents[33]. Nevertheless, denitrification can be a major source of N_2O emissions even in relatively dry soil[34], especially important when organic inputs become newly available to soil heterotrophs following direct additions of new plant residues[35] or redistribution of soil organic matter via tillage[36]. Denitrification in drier soils is typically attributed to anaerobic microsites where rates of O_2 consumption exceed diffusion, such as within soil aggregates or in microsites of active decomposition of organic substrates[20,30,37,38]. Our results show that absorption of water from the surrounding soil by plant residue fragments is an alternative

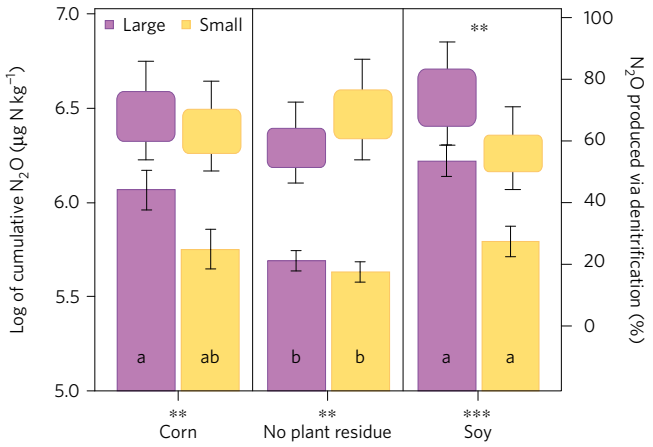

Figure 3 | Cumulative N_2O emitted during 110 days (bars) and proportion of N_2O generated by denitrification during 7 days of incubation (boxes). Data are means for plant residue and pore treatments averaged across both levels of WFPS and agricultural practices, error bars indicate s.e.m. ($n = 12$), asterisks represent statistically significant differences between small and large pores within plant types (** $p < 0.05$ and *** $p < 0.01$), and different letters represent significant differences between plant types within pore classes ($p < 0.05$). The upper and lower boundaries of the boxes indicate maximum and conservative estimates of the percentage of N_2O derived from denitrification.

previously unrecognized cause for the formation of local anaerobic conditions in relatively dry soil. The findings suggest that this mechanism can be a major contributor to microscale anaerobic heterogeneity and thus to denitrifier-derived N_2O fluxes.

Our evaluation of the microbial origin of N_2O on the basis of SP analysis within control microcosms is consistent with conventional expectations. That is, more N_2O was produced via denitrification in wetter soil (Supplementary Table 2) and in the small-pore microcosms (Fig. 3), where lower gas diffusivity enhanced O_2 limitations and greater presence of available C due to soil crushing and sieving[39,40] further enhanced denitrification (Supplementary Table 3)[6,41]. In contrast, in the microcosms with plant residues, soil moisture did not affect the proportion of N_2O produced via denitrification, and N_2O production via denitrification was greater in large than in small-pore microcosms.

Large-pore microcosms of this study were dominated by pores >35 μm in diameter and their pattern of water distribution resulted in a very substantial volume of large connected air-filled pores (Supplementary Fig. 1) with high gas diffusivity (Supplementary Table 1). The small-pore microcosms, in contrast, were dominated by 4–10 μm pores and had lower gas diffusivity.

In the large-pore microcosms there was a rapid supply of O_2 to the plant residue and no indication of O_2 shortage even during the first 4 days of the incubation when the most active decomposition of residue was taking place and N_2O emissions were high (Fig. 4). In the small-pore microcosms, O_2 levels decreased substantially, with the greatest decrease observed in the microcosms with soybean residue followed by the microcosms with corn residue. The spatial pattern of the decrease was associated with plant residue position, and, as expected[42,43], the greatest decrease in O_2 levels was observed in close proximity to the residue.

Considering the high water content of plant residue in the large-pore microcosms, which exceeded 180% even in the 30% WFPS soil, the most parsimonious explanation for this pattern is that the plant residue itself served as a local anaerobic hotspot for denitrification. Rapid mineralization under auspiciously moist conditions within the residue led to prompt O_2 consumption, while high moisture levels within the residue limited O_2 inflow. Thus, plant residue fragments adjacent to large pores provided a perfect environment for the close spatial coupling of decomposition, nitrification, denitrification and N_2O escape, ultimately leading to high rates of N_2O production and emission. Worth noting is that management practice had relatively minor effect on N_2O emissions (Fig. 3 and Supplementary Fig. 2), despite expectations, indicating that soil PSD parameters were more important than soil history for controlling N_2O emissions.

Large pores drive fate of N_2O produced within hotspots

High soil N_2O emissions stem both from N_2O production and from transport conditions conducive to N_2O escape to the atmosphere prior to its reduction to N_2 (refs 41,44–47). Our observations suggest that in plant residue-induced hotspots the PSD of the surrounding soil is crucial for enabling N_2O escape; and the greater is N_2O hotspot production the greater will be the impact of large pores on maximizing emissions, as in our soybean microcosms. Due to their low C/N ratio (Supplementary Table 4), soybean leaves decomposed very rapidly, such that >87% of their volume was lost by day 7 in large- and small-pore treatments alike (Fig. 2). Nevertheless, both the total amounts of N_2O emitted and the temporal patterns of the emissions differed between large- and small-pore soybean microcosms. The greatest plant residue-induced N_2O emission from the large-pore soybean microcosms occurred on day 3 (Fig. 5); and while in the small-pore soybean microcosms there was a relatively small increase in emission on day 3, emissions were substantially greater on day 7 when most of the soybean residue was already decomposed.

These results point to delays between N_2O production and its emission. The low gas diffusivity of the small-pore microcosms not only delayed the timing of peak emissions but also appeared to have led to reductions in the total amount of N_2O emitted. Given similar magnitudes of soybean residues decomposed in both the large- and small-pore microcosms (Fig. 2), it is likely that comparable amounts of N_2O were produced in both as well. Considering that the amount of N_2O emitted during the entire incubation in large-pore soybean microcosms was almost double that in the small-pore ones (575 versus 332 μg N kg^{-1}, respectively; Fig. 3), we can presume that the delay of emissions in the small-pore microcosms possibly led to a greater proportion of N_2O reduction to N_2.

While we did not directly evaluate the reduction of N_2O, our findings suggest that the lack of large pores created additional anaerobic areas around the decomposing residue, facilitating N_2O reduction to N_2 (Fig. 4). Because decomposition of corn residue was slower than soybean, there was also probably a smaller discrepancy between N_2O production and emission rates in small-pore samples, explaining the lack of differences in temporal patterns of large- and small-pore samples with corn.

Concluding remarks

Our results demonstrate that since most of the hotspot N_2O production took place within plant residue, the conditions within the residue itself, and not those of the bulk soil, affected N_2O production the most, while large pores in the vicinity facilitated both residue mineralization (Fig. 2) and rapid escape of produced N_2O (Fig. 5). Water uptake by plant residue from the surrounding soil enabled decomposition of the residue and N_2O production even when the adjacent soil was relatively dry. Importantly, plant residue water absorption depended on the pore characteristics of the surrounding soil, specifically on its water retention capacity: more water was absorbed by plant residue in soils where large pores predominated as compared with soil with small pores. We believe these results are generalizable to soils elsewhere, and thus suggest a promising new route for improving predictions of N_2O emissions from soil—to consider joint effects of soil PSD along with the presence and spatial distribution patterns of plant residues.

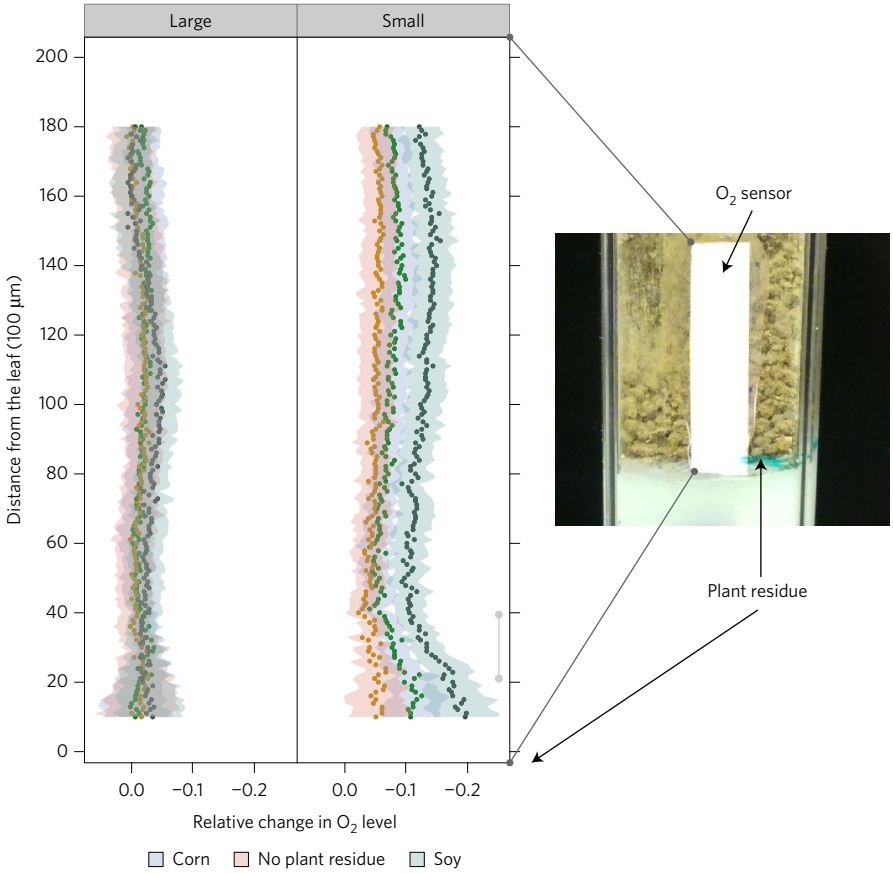

Figure 4 | Relative changes in O_2 during the first 4 days of soil microcosm incubations. On the *y* axis is the distance along the oxygen sensor from the leaf (0) to the top of the soil sample (20,000 µm); on the *x* axis are the relative cumulative changes in O_2 levels as compared with pre-incubation for large- and small-pore microcosms, respectively. The dots represent means, the shaded areas indicate s.e.m., the vertical grey bar marks the position along the sensor where there was a significant difference between microcosms with soybean leaves and microcosms with no leaves ($p < 0.05, n = 3$).

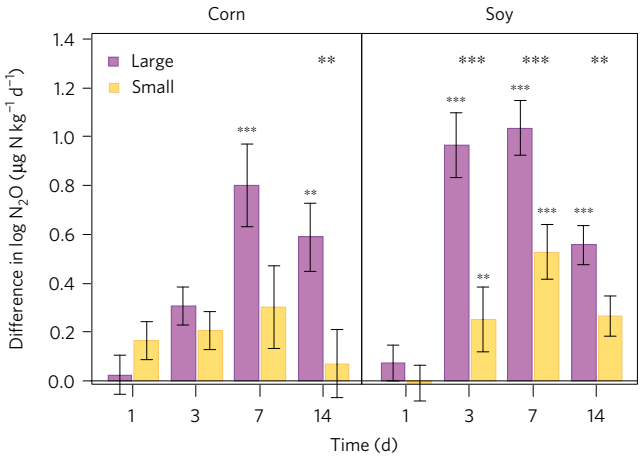

Figure 5 | Differences in N_2O emission rates between soil microcosms with plant residues and control soil during 1–14 days of incubation. Data are mean differences for plant residue and pore treatments averaged across both levels of WFPS and agricultural practices, error bars indicate s.e.m. ($n = 16$), small asterisks on top of error bars mark the differences that were significantly greater than zero, large asterisks above bars indicate significant differences between large and small pores within each plant residue type and time point (**$p < 0.05$ and ***$p < 0.01$).

Corn and soybean are among the most widely grown row crops worldwide, and plant residue incorporation is among the most commonly used agriculture practices, sometimes promoted as an effective climate change mitigation strategy due to soil carbon accretion[48]. Evidence here, however, suggests that residue incorporation should in many cases promote N_2O emissions, as has been measured elsewhere *in situ*[3], counteracting the climate benefit of soil carbon storage. Our identification of the underlying cause for this accelerated N_2O production should provide a means to design cropping practices to avoid this trade-off, in addition to providing the basis for more accurately representing N_2O fluxes in quantitative models and thus improving our understanding and estimates of this globally important gas.

Methods

Methods, including statements of data availability and any associated accession codes and references, are available in the online version of this paper.

Received 4 February 2017; accepted 4 May 2017; published online 5 June 2017

References

1. Groffman, P. M. *et al*. Challenges to incorporating spatially and temporally explicit phenomena (hotspots and hot moments) in denitrification models. *Biogeochemistry* **93,** 49–77 (2009).
2. McClain, M. E. *et al*. Biogeochemical hot spots and hot moments at the interface of terrestrial and aquatic ecosystems. *Ecosystems* **6,** 301–312 (2003).
3. Chen, H. H., Li, X. C., Hu, F. & Shi, W. Soil nitrous oxide emissions following crop residue addition: a meta-analysis. *Glob. Change Biol.* **19,** 2956–2964 (2013).
4. Li, X. X., Petersen, S. O., Sorensen, P. & Olesen, J. E. Effects of contrasting catch crops on nitrogen availability and nitrous oxide emissions in an organic cropping system. *Agric. Ecosyst. Environ.* **199,** 382–393 (2015).

5. Petersen, S. O., Mutegi, J. K., Hansen, E. M. & Munkholm, L. J. Tillage effects on N_2O emissions as influenced by a winter cover crop. *Soil Biol. Biochem.* **43,** 1509–1517 (2011).
6. Sanz-Cobena, A. *et al*. Do cover crops enhance N_2O, CO_2 or CH_4 emissions from soil in Mediterranean arable systems? *Sci. Tot. Environ.* **466,** 164–174 (2014).
7. Shcherbak, I., Millar, N. & Robertson, G. P. Global metaanalysis of the nonlinear response of soil nitrous oxide (N_2O) emissions to fertilizer nitrogen. *Proc. Natl Acad. Sci. USA* **111,** 9199–9204 (2014).
8. Gelfand, I., Shcherbak, I. I., Millar, N., Kravchenko, A. N. & Robertson, G. P. Long-term nitrous oxide fluxes in annual and perennial agricultural and unmanaged ecosystems in the upper Midwest USA. *Glob. Change Biol.* **22,** 3594–3607 (2016).
9. Butterbach-Bahl, K., Baggs, E. M., Dannenmann, M., Kiese, R. & Zechmeister-Boltenstern, S. Nitrous oxide emissions from soils: how well do we understand the processes and their controls? *Phil. Trans. R. Soc. B* **368,** 1621 (2013).
10. Ciais, P. *et al*. in *Climate Change 2013: The Physical Science Basis* (eds Stocker, T. F. *et al*.) (IPCC, Cambridge Univ. Press, 2013).
11. Forster, P. in *Climate Change 2007: The Physical Science Basis* (ed. Solomon, S.) (IPCC, Cambridge Univ. Press, 2007).
12. Kravchenko, A. N. & Robertson, G. P. Statistical challenges in analyses of chamber-based soil CO_2 and N_2O emissions data. *Soil Sci. Soc. Am. J.* **79,** 200–211 (2015).
13. Ambus, P. & Robertson, G. P. Automated near-continuous measurement of carbon dioxide and nitrous oxide fluxes from soil. *Soil Sci. Soc. Am. J.* **62,** 394–400 (1998).
14. Barton, L. *et al*. Sampling frequency affects estimates of annual nitrous oxide fluxes. *Sci. Rep.* **5,** 15912 (2015).
15. Ruan, L. L. & Robertson, G. P. Initial nitrous oxide, carbon dioxide, and methane costs of converting conservation reserve program grassland to row crops under no-till vs. conventional tillage. *Glob. Change Biol.* **19,** 2478–2489 (2013).
16. Kuzyakov, Y. & Blagodatskaya, E. Microbial hotspots and hot moments in soil: concept & review. *Soil Biol. Biochem.* **83,** 184–199 (2015).
17. Ambus, P. & Christensen, S. Measurement of N_2O emission from a fertilized grassland - an analysis of spatial variability. *J. Geophys. Res.* **99,** 16549–16555 (1994).
18. Haider, K., Mosier, A. & Heinemeyer, O. The effect of growing plants on denitrification at high soil nitrate concentrations. *Soil Sci. Soc. Am. J.* **51,** 97–102 (1987).
19. Parkin, T. B. Soil microsites as a source of denitrification variability. *Soil Sci. Soc. Am. J.* **51,** 1194–1199 (1987).
20. Sexstone, A. J., Revsbech, N. P., Parkin, T. B. & Tiedje, J. M. Direct measurement of oxygen profiles and denitrification rates in soil aggregates. *Soil Sci. Soc. Am. J.* **49,** 645–651 (1985).
21. Ball, B. C. Soil structure and greenhouse gas emissions: a synthesis of 20 years of experimentation. *Eur. J. Soil Sci.* **64,** 357–373 (2013).
22. Jungkunst, H. F., Freibauer, A., Neufeldt, H. & Bareth, G. Nitrous oxide emissions from agricultural land use in Germany—a synthesis of available annual field data. *J. Plant Nutr. Soil Sci.* **169,** 341–351 (2006).
23. Clemens, J., Schillinger, M. P., Goldbach, H. & Huwe, B. Spatial variability of N_2O emissions and soil parameters of an arable silt loam—a field study. *Biol. Fert. Soils* **28,** 403–406 (1999).
24. Kravchenko, A. N. *et al*. Intra-aggregate pore structure influences phylogenetic composition of bacterial community in macroaggregates. *Soil Sci. Soc. Am. J.* **78,** 1924–1939 (2014).
25. Negassa, W. *et al*. Properties of soil pore space regulate pathways of plant residue decomposition and community structure of associated bacteria. *PLoS ONE* **10,** e0123999 (2015).
26. Wang, W., Kravchenko, A. N., Smucker, A. J. M., Liang, W. & Rivers, M. L. Intra-aggregate pore characteristics: X-ray computed microtomography analysis. *Soil Sci. Soc. Am. J.* **76,** 1159–1171 (2012).
27. Ostrom, N. E. & Ostrom, P. H. in *The Isotopomers of Nitrous Oxide: Analytical Considerations and Application to Resolution of Microbial Production Pathways* (ed. Baskara, M.) 453–476 (Springer, 2011).
28. Ostrom, N. E. & Ostrom, P. H. Mining the isotopic complexity of nitrous oxide: a review of challenges and opportunities. *Biogeochemistry* **132,** 359–372 (2017).
29. Breland, T. A. Enhanced mineralization and denitrification as a result of heterogeneous distribution of clover residues in soil. *Plant Soil* **166,** 1–12 (1994).
30. Loecke, T. D. & Robertson, G. P. Soil resource heterogeneity in terms of litter aggregation promotes nitrous oxide fluxes and slows decomposition. *Soil Biol. Biochem.* **41,** 228–235 (2009).
31. Magid, J., De Neergaard, A. & Brandt, M. Heterogeneous distribution may substantially decrease initial decomposition, long-term microbial growth and N-immobilization from high C-to-N ratio resources. *Eur. J. Soil Sci.* **57,** 517–529 (2006).
32. Markfoged, R., Nielsen, L. P., Nyord, T., Ottosen, L. D. M. & Revsbech, N. P. Transient N_2O accumulation and emission caused by O_2 depletion in soil after liquid manure injection. *Eur. J. Soil Sci.* **62,** 541–550 (2011).
33. Davidson, E. A., Keller, M., Erickson, H. E., Verchot, L. V. & Veldkamp, E. Testing a conceptual model of soil emissions of nitrous and nitric oxides. *Bioscience* **50,** 667–680 (2000).
34. Robertson, G. P. & Tiedje, J. M. Nitrous-oxide sources in aerobic soils—nitrification, denitrification and other biological processes. *Soil Biol. Biochem.* **19,** 187–193 (1987).
35. Li, X. X., Sorensen, P., Olesen, J. E. & Petersen, S. O. Evidence for denitrification as main source of N_2O emission from residue-amended soil. *Soil Biol. Biochem.* **92,** 153–160 (2016).
36. Ostrom, N. E. *et al*. Isotopologue data reveal bacterial denitrification as the primary source of N_2O during a high flux event following cultivation of a native temperate grassland. *Soil Biol. Biochem.* **42,** 499–506 (2010).
37. Petersen, S. O., Ambus, P., Elsgaard, L., Schjonning, P. & Olesen, J. E. Long-term effects of cropping system on N_2O emission potential. *Soil Biol. Biochem.* **57,** 706–712 (2013).
38. Zhu, K., Ruun, S., Larsen, M., Glud, R. N. & Jensen, L. S. Heterogeneity of O_2 dynamics in soil amended with animal manure and implications for greenhouse gas emissions. *Soil Biol. Biochem.* **84,** 96–106 (2015).
39. Adu, J. K. & Oades, J. M. Utilization of organic materials in soil aggregates by bacteria and fungi. *Soil Biol. Biochem.* **10,** 117–122 (1978).
40. Hassink, J. Effects of soil texture and structure on carbon and nitrogen mineralization in grassland soils. *Biol. Fert. Soils* **14,** 126–134 (1992).
41. Pimentel, L. G., Weiler, D. A., Pedroso, G. M. & Bayer, C. Soil N_2O emissions following cover-crop residues application under two soil moisture conditions. *J. Plant Nutr. Soil Sci.* **178,** 631–640 (2015).
42. Jacinthe, P. A., Groffman, P. M., Gold, A. J. & Mosier, A. Patchiness in microbial nitrogen transformations in groundwater in a riparian forest. *J. Environ. Qual.* **27,** 156–164 (1998).
43. Jorgensen, B. B. & Revsbech, N. P. Diffusive boundary-layers and the oxygen-uptake of sediments and detritus. *Limnol. Oceanogr.* **30,** 111–122 (1985).
44. Balaine, N. *et al*. Changes in relative gas diffusivity explain soil nitrous oxide flux dynamics. *Soil. Sci. Soc. Am. J.* **77,** 1496–1505 (2013).
45. Clough, T. J., Sherlock, R. R. & Rolston, D. E. A review of the movement and fate of N_2O in the subsoil. *Nutr. Cycl. Agroecosyst.* **72,** 3–11 (2005).
46. Liengaard, L. *et al*. Hot moments of N_2O transformation and emission in tropical soils from the Pantanal and the Amazon (Brazil). *Soil Biol. Biochem.* **75,** 26–36 (2014).
47. Rabot, E., Henault, C. & Cousin, I. Effect of the soil water dynamics on nitrous oxide emissions. *Geoderma* **280,** 38–46 (2016).
48. Lal, R. Residue management, conservation tillage and soil restoration for mitigating greenhouse effect by CO_2-enrichment. *Soil Tillage. Res.* **43,** 81–107 (1997).

Acknowledgements

We are indebted to K. Kahmark for conducting N_2O analyses; to H. Gandhi and J. Haslun for conducting site-preference measurements; and to the KBS LTER team for agronomic management of the field experiment. Funding has been provided by the National Science Foundation's Long-Term Ecological Research Program (DEB 1027253), by the National Science Foundation's Geobiology and Low Temperature Geochemistry Program (Award no. 1630399), by the Department of Energy Great Lakes Bioenergy Research Center (DOE Office of Science BER DE-FC02-07ER64494), by Michigan State University's AgBioResearch (Project GREEEN), and by Michigan State University's Discretionary Funding Initiative. Portions of this work were performed at GeoSoilEnviroCARS (The University of Chicago, Sector 13), Advanced Photon Source (APS), Argonne National Laboratory. GeoSoilEnviroCARS is supported by the National Science Foundation - Earth Sciences (EAR-1128799) and Department of Energy—GeoSciences (DE-FG02-94ER14466).

Author contributions

A.N.K. developed concepts, conducted data analyses and wrote the paper. E.R.T. designed, led and conducted the research, and contributed to writing. A.K.G. and N.E.O. contributed to development of research concepts, research conduct and writing. J.Y., K.A. and M.L.R. contributed to research conduct. G.P.R. contributed to the development of research concepts and writing.

Additional information

Supplementary information is available in the online version of the paper. Reprints and permissions information is available online at www.nature.com/reprints. Publisher's note: Springer Nature remains neutral with regard to jurisdictional claims in published maps and institutional affiliations. Correspondence and requests for materials should be addressed to A.N.K.

Competing financial interests

The authors declare no competing financial interests.

Methods

Soil sampling and preparation. Soil samples were collected from conventionally and organically managed corn–soybean–wheat rotation treatments in the Main Cropping System Experiment of the Kellogg Biological Station Long-Term Ecological Research site (KBS LTER). Soils are Typic Alfisols of Kalamazoo and Oshtemo series, with properties common to the deciduous forest zone of the US Midwest and Europe. The conventional treatment obtains agrochemical inputs consistent with recommendations of Michigan State University Extension. The organic treatment does not receive any chemical inputs but includes cover crops (cereal rye and red clover) as part of the rotation. Additional climate, soils and agronomic details are available elsewhere[49]. KBS LTER was established in 1989 and since then the organic management has resulted in greater soil C levels than the conventional management[50,51].

Soil samples were collected in autumn of 2014, after corn harvest, from 0–15 cm depth, representing the Ap horizon. Air-dried samples were used to prepare soil materials of two contrasting pore characteristics, with predominantly large and small pores, respectively (Supplementary Fig. 1). The large-pore material was obtained by sieving air-dry soil and collecting the 1–2 mm sieved fraction. To minimize inherent differences, the small-pore material was created from the large-pore material. For that, the large-pore material was crushed and sieved, and the 0.05–0.1 mm fraction so-produced was collected for the experiments. By design, the large- and small-pore materials had very substantial differences in their PSD. Despite their identical origin, crushing and sieving had unavoidable effects on particle-size distributions of the materials and on the availability of soil C to decomposers[39,40] (Supplementary Table 3).

Soil microcosms. Soil microcosms (8 mm diameter × 10 mm height) were constructed using the two soil materials. We constructed the microcosms with dry corn and soybean leaves (Supplementary Fig. 3) and also control microcosms without leaves. All samples were constructed so as to maintain the same bulk density of 1.1 g cm^{-3}; thus, all treatments had the same 58% total porosity.

Leaf disc preparation. Corn and soybean were harvested 75 d after germination. Leaf discs (⌀ 7 mm) were prepared by cutting the leaves into circles using a hole punch. The leaf discs were then flat dried in a herbarium drying press. The weight of each individual leaf disc was recorded before it was placed into the microcosm (Supplementary Table 4).

Incubation experiment. Microcosms were incubated at two soil moisture levels corresponding to water-filled pore spaces (WFPS) of 30% and 45% (Supplementary Table 1). These WFPS levels reflected the following hydrological characteristics of the studied soil: WFPS of 30% corresponded to the porosity of 1–2 mm soil fraction used in this study—that is, the condition at which large pores were not filled with water, and, thus, served as conduits for free gas diffusion. WFPS of 45% corresponded to the field capacity of the microcosms made of 1–2 mm soil fraction, the state when capillary menisci between soil aggregates were expected to restrict free gas flow. The porosity of 1–2 mm fraction fragments was assessed from X-ray μ-CT images, whereas the field capacity was measured by free drainage of water-saturated microcosms.

Relevant amounts of water were added separately to the bottom and top parts of the microcosm during its construction to ensure even soil moisture distribution through the entire sample. Each microcosm unit was placed into a 40 ml test tube containing 1 ml water and capped with a stopper. Four replicated microcosm samples were incubated for each of the 24 experimental treatments (3 substrate levels (corn, soybean, control) × 2 agricultural systems × 2 pore sizes × 2 soil moisture levels) for a total of 96 microcosms. The samples were incubated for 110 days, during which the headspace was sampled on days 1, 3, 7, 14 and thereafter every 12 days, for a total of 11 sampling events. At each sampling event, the headspace gas was sampled into pre-evacuated 5 ml Exetainers and analysed for N_2O using an Agilent 7890 GC equipped with flame ionization and electron capture detectors.

Moisture levels in leaf discs. To determine gravimetric moisture contents of leaf discs during the incubation we conducted a supplementary experiment with a separate set of microcosms created using air-dried leaves as described above. Soil from conventional management practice was used in this analysis. The microcosms were allowed to equilibrate with added water for 4 h, a time adequate for complete water redistribution through the microcosm, yet sufficiently short to preclude measurable leaf decomposition. Then we disassembled the microcosms, weighed the leaf discs, and calculated gravimetric water content of each leaf. In cases when there was soil attached to wet leaves, the leaves were weighed and dried and the amount of attached soil was determined by weighing the dry soil separated from the leaves, and then subtracted.

X-ray μ-CT scanning and image analyses. For image analysis, an additional set of microcosms with corn and soy leaves were subjected to incubations and scanned at day 7, 14 and 24. Scanning was destructive: that is, to ensure higher accuracy in estimating leaf sizes, prior to scanning the samples were air-dried and thus not used in further incubations. We scanned 1–3 replicates for each of the 48 treatment × day combinations (2 substrate levels (corn, soybean) × 2 agricultural systems × 2 pore sizes × 2 soil moisture levels × 3 sampling dates), for a total of 71 scanned microcosm samples. X-ray μ-CT scanning was conducted on the bending magnet beam line, station 13-BM-D of the GeoSoilEnvironCARS at the Advanced Photon Source, Argonne National Laboratory, with resolutions 3–6 μm (ref. 52). Quantification of the plant leaf volume within each microcosm was conducted using image segmentation and particle analysis tools available in ImageJ (http://rsbweb.nih.gov/ij)[25,53]. To obtain detailed pore characteristics of the created soil materials a subset of samples was scanned at 2 μm resolution. In the samples from the subset, pores were identified using the indicator kriging method[54,55] and their size distributions were obtained using a medial axis approach implemented in 3DMA-Rock software[56,57]. To visualize the location of the water added to the microcosms, we prepared a subset of control samples using 10% KI solution. The samples were scanned at 2 μm resolution at two energy levels, namely, 33.269 keV, which is above the iodine K absorption edge and 33.108, which is below the edge. The two data sets were subtracted, which clearly identifies the location of the iodine and hence the liquid added to the system.

Spatial pattern in O_2 distribution. A supplementary experiment was conducted to assess the spatial patterns in O_2 distribution within the samples using optical oxygen sensors (optodes). The non-invasive sensors measure partial pressure of O_2 by recording fluorescence quenching, where oxygen quenches a photoluminescent substance (for example, ruthenium(II)-diimine-complex or platinum(II)-porphyrin)[58]. The sensor foil (SF-PSt3- NAU-YOP, PreSens, Precision Sensing GmbH), 2 × 0.5 cm, was glued to the inner side of the container with the microcosm sample and the leaves placed at the bottom of the microcosms (Fig. 4). The sensor signal was read every 20 min for 4 days from the start of the incubation. To reduce noise, the original 25-μm-resolution measurements were aggregated to 100 μm resolution. Relative deviation of O_2 levels from the pre-incubation average was used to asses O_2 changes.

Gas diffusivity calculations. The information on pore volumes inside and between soil fragments and their air-filled status obtained using X-ray μ-CT was used to estimate relative gas diffusion coefficients in the microcosms. We used an approach based on the conceptual model of a bimodal porous medium developed by Resurreccion and colleagues[59]. The ratio between the gas diffusion coefficients in the soil, D_p, and in the free air, D_o, changes with soil air content as:

$$\frac{D_p}{D_o} = \begin{cases} \left(\frac{\varepsilon_1}{\Phi_1}\right)^{N_1} \varepsilon_1^{X_1} & \varepsilon \le \Phi_1 \\ \Phi_1^{X_1} + F_2 \varepsilon_2^{X_2} & \varepsilon > \Phi_1 \end{cases} \quad (1)$$

where Φ_1 is the inter-clod porosity (cm^3 cm^{-3}); ε_1, ε_2 and ε are the inter-clod and intra-clod, and total air-filled porosities, respectively (cm^3 cm^{-3}); X_1 and X_2 are the dry-region pore connectivity factors of inter- and intra-clod pores (dimensionless); and N_1 and F_2 are the empirical parameters (dimensionless).

Parameters of equation (1) were set on the basis of studies by Currie[60,61] as $X_1 = 1.56$, $N_1 = 1.82$ for the 0.05–0.1 mm aggregate fraction, and $X_1 = 1.73$, $X_2 = 1.21$ and $F_2 = 0.71$ for the 1–2 mm aggregate fraction, respectively.

SP analysis. The relative importance of bacterial denitrification (including nitrifier-denitrification) to total N_2O production was determined as described by Ostrom and colleagues[36]. Pure culture studies demonstrate that SP values of 33 to 37 and −10 to 0‰, respectively, indicate N_2O production from hydroxylamine oxidation + fungal denitrification and bacterial denitrification[62,63]. On the basis of these values the proportion of N_2O derived from denitrification can be determined from the SP value of soil-derived N_2O (ref. 27). As ambient air was used as the headspace in our soil microcosms, the SP of soil-derived N_2O was calculated on the basis of the isotope values for ambient air (in blanks) and headspace gas analysed at the end of the 7 day incubation period[27]. SP was determined only on incubations lasting 7 days, the period of time that encompassed the highest rates of N_2O production. To obtain sufficient N_2O for isotope analyses larger microcosms (⌀ 25 mm × 10 mm) were prepared following the same procedures as described above. The N_2O obtained from microcosms was analysed using a Trace Gas System (Elementar) interfaced to an Elementar Isoprime 100 mass spectrometer for determination of bulk $\delta^{15}N$, $\delta^{18}O$ and SP[62,63]. Within the Trace Gas System, water and CO_2 are removed using chemical scrubbers (magnesium perchlorate and Carbosorb, respectively) and N_2O is chromatographically separated from the residual CO_2 on a Porapak Q column that is interfaced to the mass spectrometer[62,63]. The Isoprime multi-collector mass spectrometer simultaneously monitors 5 masses of interest for N_2O isotopomers: 30, 31, 44, 45 and 46. We follow the convention of Toyoda and Yoshida[64] in defining the central and outer nitrogen atoms as α and β, respectively. We applied corrections for the contribution of ^{17}O to masses 31 and 45 and for a small degree of rearrangement of ^{15}N between the α and β positions within the ion source[64].

Statistical analysis. Data analyses were conducted using the PROC MIXED procedure of SAS (SAS, 2012). For one-time measurements, for example, cumulative amounts of emitted N_2O, the statistical model included fixed effects of the studied factors and their interactions and the random effect of the experimental blocks. The studied factors were agricultural management practices, plant residue types, soil WFPS levels and soil pore size distribution treatments. For measurements that were taken at multiple times from each microcosm, for example, N_2O emission rates, the repeated measures approach was used, with individual microcosms nested within respective treatments and treated as the random effect and an error term. Normality and homogeneity of variance assumptions were assessed using plots of the residuals. Lack of normality in the N_2O data was addressed by log-transformation and unequal variance analysis was used as needed on the basis of Bayesian information criterion values[65]. Significant interaction effects were examined using analysis of simple effects, also known as slicing[66]. The differences between control microcosms and the microcosms with plant residue, also known as plant residue-induced effects, were quantified using contrast statements. Likewise, the differences between plant residue-induced effects in different treatments were assessed by contrasts. Results were reported as statistically significant at $p < 0.05$ and $p < 0.01$.

Data availability. Data collected for this study will be preserved in the KBS LTER database available at http://lter.kbs.msu.edu/datatables. Data available from the Dryad Digital Repository: http://dx.doi.org/10.5061/dryad.83150.

References

49. Robertson, G. P. & Hamilton, S. K. in *The Ecology of Agricultural Landscapes: Long-Term Research on the Path to Sustainability* (eds Hamilton, S. K., Doll, J. E. & Robertson, G. P.) 1–32 (Oxford Univ. Press, 2015).
50. Senthilkumar, S., Kravchenko, A. N. & Robertson, G. P. Topography influences management system effects on total soil carbon and nitrogen. *Soil Sci. Soc. Am. J.* **73,** 2059–2067 (2009).
51. Syswerda, S. P., Corbin, A. T., Mokma, D. L., Kravchenko, A. N. & Robertson, G. P. Agricultural management and soil carbon storage in surface vs. deep layers. *Soil Sci. Soc. Am. J.* **75,** 92–101 (2011).
52. Rivers, M. L., Sutton, S. R. & Eng, P. Geoscience applications of x-ray computed microtomography. *Dev. X-Ray Tomogr. II* **3772,** 78–86 (1999).
53. Kravchenko, A. N., Negassa, W., Guber, A. K. & Schmidt, S. New approach to measure soil particulate organic matter in intact samples using X-ray computed microtomography. *Soil Sci. Soc. Am. J.* **78,** 1177–1185 (2014).
54. Oh, W. & Lindquist, W. B. Image thresholding by indicator kriging. *IEEE Trans. Pattern Anal.* **21,** 590–602 (1999).
55. Wang, W., Kravchenko, A. N., Smucker, A. J. M. & Rivers, M. L. Comparison of image segmentation methods in simulated 2D and 3D microtomographic images of soil aggregates. *Geoderma* **162,** 231–241 (2011).
56. Lindquist, W. B., Venkatarangan, A., Dunsmuir, J. & Wong, T. F. Pore and throat size distributions measured from synchrotron X-ray tomographic images of Fontainebleau sandstones. *J. Geophys. Res.* **105,** 21509–21527 (2000).
57. Peth, S. *et al*. Three-dimensional quantification of intra-aggregate pore-space features using synchrotron-radiation-based microtomography. *Soil Sci. Soc. Am. J.* **72,** 897–907 (2008).
58. Dutta, T. *et al*. Vadose zone oxygen (O_2) dynamics during drying and wetting cycles: an artificial recharge laboratory experiment. *J. Hydrol.* **527,** 151–159 (2015).
59. Resurreccion, A. C. *et al*. Hierarchical, bimodal model for gas diffusivity in aggregated, unsaturated soils. *Soil Sci. Soc. Am. J.* **74,** 481–491 (2010).
60. Currie, J. A. Gaseous diffusion in porous media .2. Dry granular materials. *Br. J. Appl. Phys.* **11,** 318–324 (1960).
61. Currie, J. A. Gas-diffusion through soil crumbs—the effects of compaction and wetting. *J. Soil Sci.* **35,** 1–10 (1984).
62. Sutka, R. L. *et al*. Distinguishing nitrous oxide production from nitrification and denitrification on the basis of isotopomer abundances. *Appl. Environ. Microb.* **72,** 638–644 (2006).
63. Sutka, R. L., Ostrom, N. E., Ostrom, P. H., Gandhi, H. & Breznak, J. A. Nitrogen isotopomer site preference of N_2O produced by *Nitrosomonas europaea* and *Methylococcus capsulatus* Bath. *Rapid Commun. Mass Spectrom.* **18,** 1411–1412 (2004).
64. Toyoda, S. & Yoshida, N. Determination of nitrogen isotopomers of nitrous oxide on a modified isotope ratio mass spectrometer. *Anal. Chem.* **71,** 4711–4718 (1999).
65. Milliken, G. A. & Johnson, D. E. *Analysis of Messy Data Volume I: Designed Experiments* 2nd edn (Chemical Rubber Company, 2009).
66. Winer, B. J. *Statistical principles in Experimental Design* (McGraw-Hill, 1971).

nature geoscience

SUPPLEMENTARY INFORMATION

DOI: 10.1038/NGEO2963

In the format provided by the authors and unedited.

Hotspots of soil N_2O emission enhanced through water absorption by plant residue

A. N. Kravchenko*, E. R. Toosi, A.K. Guber, N. E. Ostrom, J. Yu, K. Azeem, M. L. Rivers, and G. P. Robertson

*Corresponding author:

Email: kravche1@msu.edu

Phone: 517.353.0469

This file includes:

Figures S1-S3

Tables S1-S4

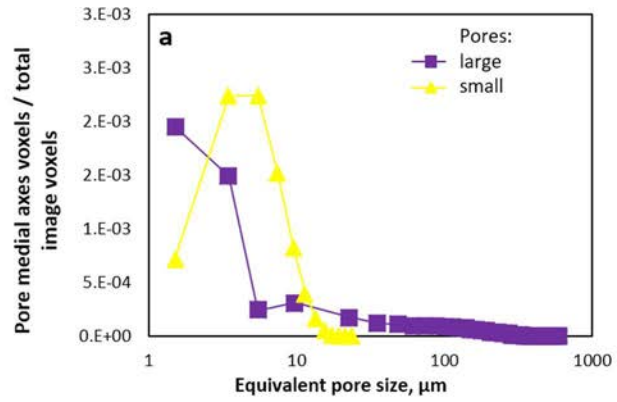

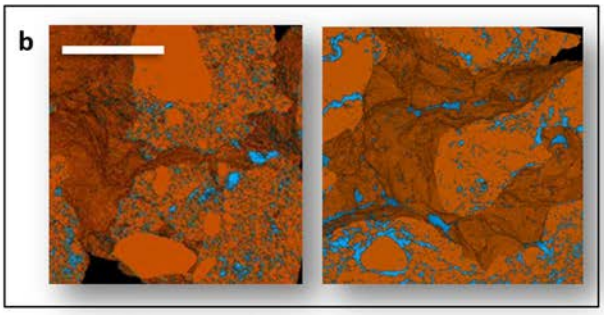

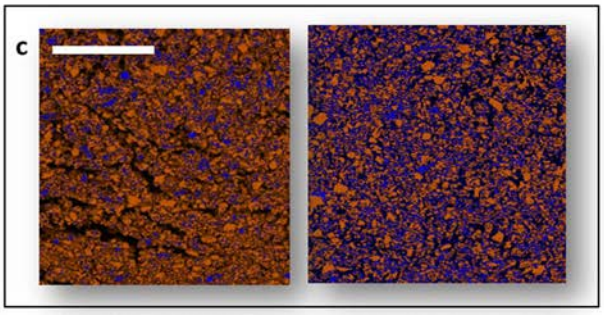

Figure 1| Pore size distributions and water distribution patterns in the studied microcosms. (a) Pore size distributions in the large and small pore samples obtained from quantification of pore median axes in 2 µm resolution 3D images via 3DMA-Rock software. Examples of **(b)** large and **(c)** small pore samples at 30% (left) and 45% (right) WFPS. Liquid (blue) is visualized using dual energy scanning with 10% KI solution. Scale bars represent 1 mm.

Figure S2 | N_2O emission rates during soil microcosm incubation. The main graph presents the effect of adding plant residue to soil microcosms (means, error bars indicate SEs, letters mark significant differences between substrate treatments at $p<0.05$, $n=4$). Inserts present effects of soil moisture (a), management history (b), and pore architecture (c) on N_2O emission during first 2-5 weeks of incubation (means, stars mark significant differences at $p<0.05$ level).

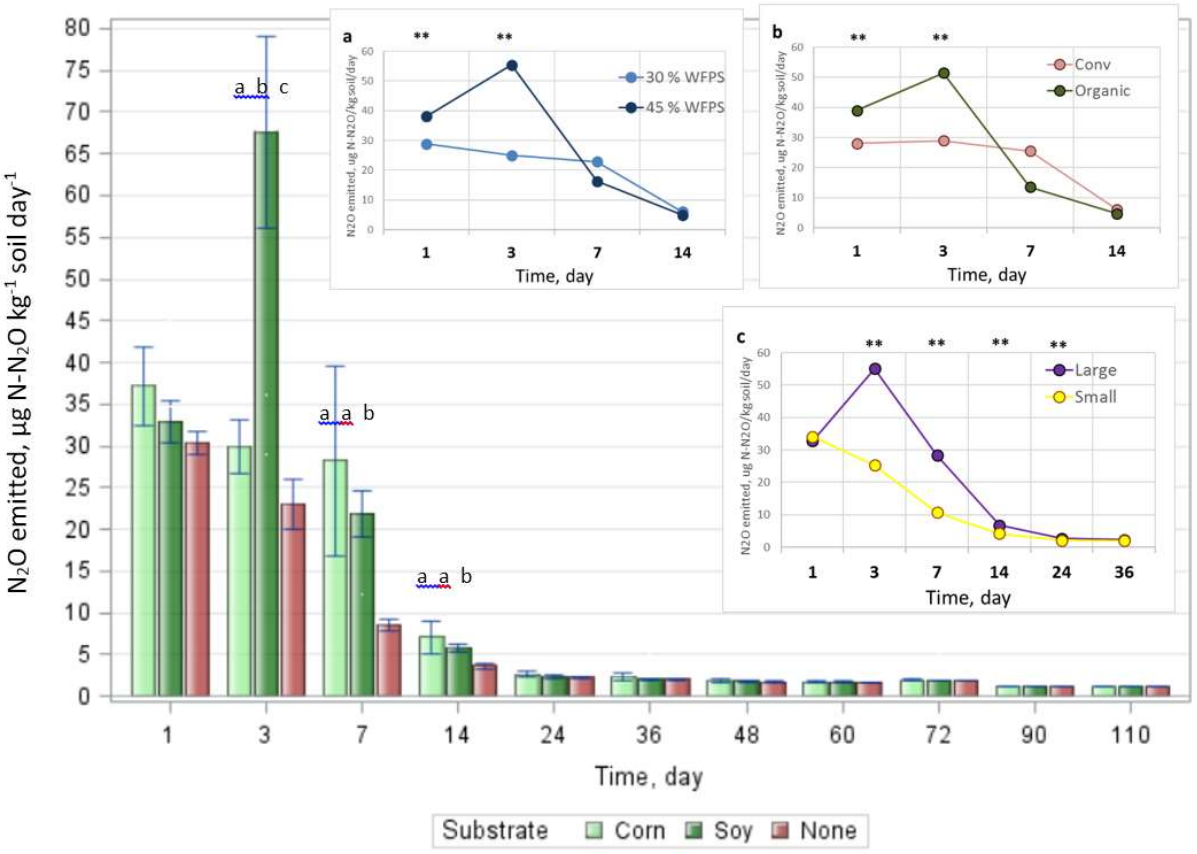

Figure S3 | Hotspot microcosm construction. (a) 3D X-ray µCT images of the microcosms with large (left) and small (right) pore materials. (b) A 0.5 g of soil material (brown) was placed in a 3 mL plastic container, moistened to one of the two studied WFPS levels and packed to bulk density of 1.1 g/cm^3. The leaf disk (green) was placed on top and the second half of the soil material was packed onto the disk and moistened. A perforated Teflon disk at the bottom of the column (yellow) retained the soil while maintaining air flow.

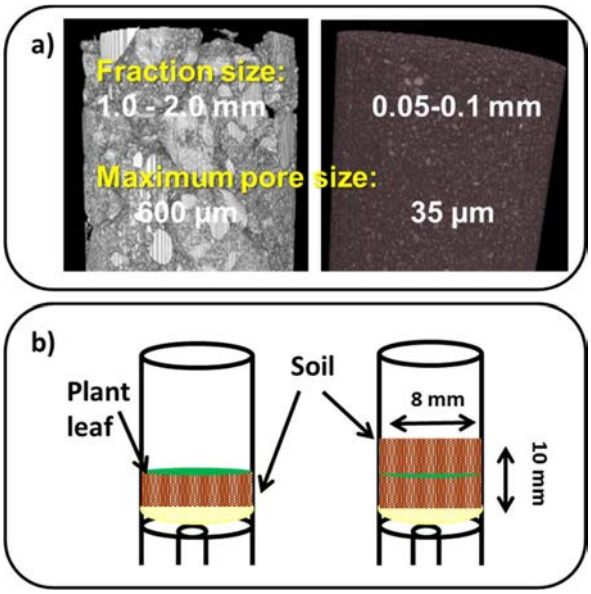

Table S1. Soil moisture content and gas diffusion settings in the large and small pore materials used in the study at 30% and 45% WFPS levels.

Pore size treatment	WFPS, %	Gravimetric soil moisture content, %	Gas diffusion coefficient, Dp/Do
Large	30	15	0.17
	45	24	0.16
Small	30	15	0.11
	45	24	0.04

Table S2. Percent of N_2O produced via denitrification in the microcosms of the two studied WFPS levels at the three substrate treatments (means averaged across both pore size treatments, standard errors are shown in parentheses, means within the same row followed by the same letter are not significantly different from each other ($p<0.05$), n=8).

Plant residue treatment	WFPS %	
	30	45
Corn	58.4 (5.0)a	65.9 (4.5)a
Soybean	67.0 (3.8)a	56.4 (6.5)a
No residue (control)	55.1 (6.2)a	66.1 (3.5)b

Table S3. Soluble organic C in the materials of the large and small pore treatments in conventional and organic agricultural managements (means, standard errors are shown in parentheses, different letters mark statistically significant differences among the treatments and managements at $P<0.05$, n=3).

Pore size treatment	Agronomic management	Soluble organic C, μgC g^{-1}soil
Large	Conventional	204 (5) a
	Organic	292 (25) b
Small	Conventional	314 (4) b
	Organic	344 (19) b

Table S4. Characteristics of corn and soybean leaves used in the incubations (means, standard errors are shown in parentheses, n=6).

Plant residue	Leaf weight, mg	C concentration, %	N concentration, %	C:N ratio	N input with leaf, mg
Corn	1.16 (0.03)	44.4 (0.1)	3.8 (0.1)	11.8 (0.2)	0.044
Soybean	1.23 (0.04)	38.6 (0.4)	5.3 (0.2)	7.4 (0.3)	0.065